Transition metal compounds with S/N-functionalized NHC ligands: structures, redox properties and electrocatalytic activity

Luo, S.; Luo S.

CHAPTER 6

Cobalt Complexes of Pyridine-Amide Functionalized Carbene Ligands as Electrocatalysts for HER

*Two pyridyl-amide substituted imidazolium salts H_2**L1**Cl and H_2**L2**Cl were synthesized and successfully employed as ligand precursors for the syntheses of novel cobalt(III) complexes [Co(**L1**)$_2$]Cl and [Co(**L2**)$_2$]Cl bearing chelating N-heterocyclic carbene (NHC) ligands. The crystal structure determination of [Co(**L1**)$_2$]PF_6 and [Co(**L2**)$_2$]Cl revealed that the central cobalt ions in both complexes are bound by two ligands binding in a meridional tridentate mode, with two dangling benzyl groups in the first compound and pyridine groups in the latter. The reversible redox properties of the two compounds were investigated using cyclic voltammetry. In dimethylformamide in presence of acetic acid the two compounds show electrocatalytic activity in proton reduction as confirmed by cyclic voltammetry and quantified with gas chromatography. Compound [Co(**L2**)$_2$]Cl equipped with two uncoordinated pyridine groups that can act as proton relay, shows higher electrocatalytic activity in HER compared with [Co(**L1**)$_2$]Cl, though a total turnover of 1.5 in 2h is barely to be announced as efficient catalyst for HER. Nevertheless, the neat compound synthesis method and good stability of the compounds in acid might be a merit.*

This chapter will be published: S. Luo, M.A. Siegler, and E. Bouwman, manuscript in preparation

6.1 Introduction

The design of molecular electrocatalysts for the hydrogen evolution reaction (HER) is one of the important research topics of the last decade. In 2007, DuBois's research group reported a class of nickel complexes comprising chelating phosphane ligands with pendant nitrogen bases showing excellent electrocatalytic activity for the hydrogen evolving reaction (HER).[1] Since then, the development of functional models for the active site of hydrogenases to be applied as electrocatalysts for the HER has been receiving increasing attention. Apart from the aforementioned Ni-diphosphane catalysts, a number of other new classes of electrocatalysts with outstanding activity in the HER have been reported, i.e. the cobaloxime catalysts,[2, 3] and polypyridyl-based catalyst with first row transition metals, e.g. Co, Cu, Ni and Fe.[4-7] Cobalt as one of the inexpensive transition metals, receives considerable attention in the design molecular catalyst.[2-5] N-heterocyclic carbene (NHC) ligands have been extensively studied in transition metal coordination chemistry with applications in homogeneous catalysis,[8, 9] but so far this kind of strong σ donor ligands has not been widely used to design electrocatalysts for the HER. In recent years only a few Co-NHC complexes have been reported as electrocatalysts for the HER.[10, 11]

In this chapter, the synthesis and characterization is reported of two new cobalt(III)-NHC complexes, which show electrocatalytic activity in the HER in dimethylformamide using acetic acid as the proton source. Their catalytic activity is compared with the related Ni-NHC complexes that are discussed in Chapter 5, with the aim to study the influence of different transition metal ions on the redox potentials and catalytic activity in the HER.

6.2 Results and Discussion

6.2.1 Synthesis of the complexes

The new Co-NHC compounds $[Co(\mathbf{L1})_2]Cl$ and $[Co(\mathbf{L2})_2]Cl$ were prepared by reacting the ligand precursors[12] with anhydrous cobalt(II) acetate in acetonitrile or DMF in the presence of K_2CO_3. The following workup procedure was done in an air atmosphere, and the compounds were obtained as brown solids in a yield of 25% and 30%, respectively (Figure 6.1). Attempts were undertaken to synthesize complexes with a 1:1 metal-to-ligand ratio by varying the ratios of the starting materials. However, only the $[Co(\mathbf{Lx})_2]Cl$ type complexes were obtained, which were characterized with X-ray diffraction and mass spectrometry. Although a cobalt(II) salt was used in the complex synthesis, the formation of cobalt(III) complexes was apparent by the diamagnetic ^1H NMR spectra of the obtained compounds (Figure AVI.1). The ESI-MS spectra of both cobalt complexes exhibit base peaks corresponding to the $[M - Cl]^+$ cations (Figure AVI.2).

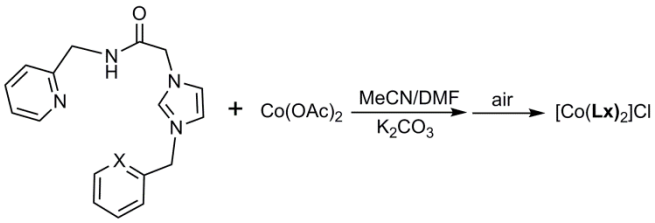

*Figure 6.1. Synthetic route of the complexes [Co(**L1**)$_2$]Cl and [Co(**L2**)$_2$]Cl.*

6.2.2 Structural characterization of the complexes

It appeared to be difficult to obtain single crystals suitable for X-ray structure determination. Needle-shaped single crystals of [Co(**L2**)$_2$]Cl were obtained from DCM; however, the counter ion appeared to be extremely disordered, making the crystallographic refinement unsatisfactory. Block-shaped crystals were obtained from a mixture of MeCN/H_2O, but the crystal that was mounted on the diffractometer appeared not to be a single crystal, but rather a composite of two crystals related by a rotation. Fortunately the diffraction data obtained with this crystal are satisfactory for crystallographic refinement. The crystallographic and refinement data are provided in Table AVI.1. For complex [Co(**L1**)$_2$]Cl it also appeared difficult to obtain single crystals. Thus, anion exchange was performed by adding a solution of the complex [Co(**L1**)$_2$]Cl in acetonitrile to a boiling acetonitrile solution of NH_4PF_6. Orange-colored, block-shaped crystals were obtained within one week; unfortunately, again part of the PF_6^- anion as well as co-crystallized solvent molecules appeared to be severely disordered. It is assumed that the flexible benzyl arm in [Co(**L1**)$_2$]Cl hampers crystallization of this compound. Similar problems have been reported for the structures of a number of Co^{III}-NHC complexes because of the disorder of counter ions.[10, 13] The general structure of the cationic complex in [Co(**L1**)$_2$]Cl could be reliably determined from the difference Fourier maps. Projections of the [Co(**L1**)$_2$]$^+$ and [Co(**L2**)$_2$]$^+$ cations are shown in Figure AVI.3 and Figure 6.2, respectively. Selected bond distances and angles are provided in Table AVI.2.

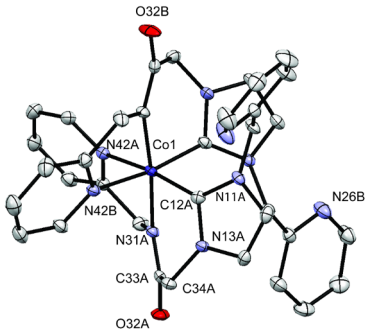

*Figure 6.2. Displacement ellipsoid plots of the cationic complex in [Co(**L2**)$_2$]Cl, drawn at 50% probability level with selected atom numbering. For clarity the hydrogen atoms, chloride ion and the lattice water molecules are omitted.*

The projection of $[Co(\mathbf{L1})_2]PF_6$ reveals that the central cobalt ion is coordinated by two ligands bound in a tridentate fashion. The meridional binding of the ligand is largely dictated by the sp^2 hybridization of the amide nitrogen atom. The Co–C and Co–N bond lengths are slightly longer than the related distances found in the nickel compounds described in Chapter 5. The Co–C bond lengths are similar to those in reported Co-carbene complexes.[13-18] $[Co(\mathbf{L2})_2]Cl$ presents a similar coordination sphere for the central cobalt ion as in $[Co(\mathbf{L1})_2]PF_6$, with two uncoordinated methylpyridine groups instead of benzyl groups.

6.2.3 Electrochemical properties of the complexes

The electrochemical properties of the two complexes have been investigated using cyclic voltammetry (CV) in DMF solutions. For the complex $[Co(\mathbf{L1})_2]Cl$, two reversible redox couples appeared with $E_{1/2}$ at −1.19 V and −1.84 V vs. Ag/AgCl. Similarly, for complex $[Co(\mathbf{L2})_2]Cl$ two redox waves were found at approximately the same potentials (Figure 6.3, Table 6.1). In addition, in the voltammogram of $[Co(\mathbf{L2})_2]Cl$ two small irreversible reductive waves were found at −1.66 V and −2.00 V. As the CVs of the ligand precursors do not show redox activity at these potentials (see Appendix VI, Figure AVI.5), it is assumed that the two reversible or quasi-reversible events are metal-centered. Thus, these two processes are tentatively assigned to the Co^{III}/Co^{II}, and Co^{II}/Co^{I} redox couples. Depending on the coordinating ligands and coordination geometry, the Co^{III}/Co^{II} and Co^{II}/Co^{I} redox potentials can be largely different, ranging from 1.40 V to −0.83 V for Co^{III}/Co^{II} and −0.23 V to −1.38 for Co^{II}/Co^{I} vs. Ag/AgCl.[10, 11, 14] The redox potentials of the cobalt(III) compounds reported in this Chapter appear to be more negative by nearly 0.5 V comparing to the potentials in literatures,[10, 11, 14] most likely because of the highly electron-donating nature of the carbene ligands.

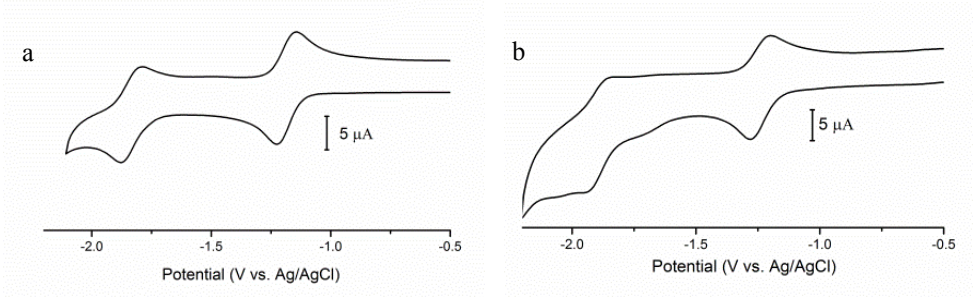

Figure 6.3. CVs of 1 mM (a) complex $[Co(\mathbf{L1})_2]Cl$ and (b) $[Co(\mathbf{L2})_2]Cl$ in DMF containing 0.1 M TBAP as electrolyte at scan rate 0.1 V/s, using glassy carbon working electrode.

Table 6.1. Electrochemical data of the cobalt compounds.[a]

	E_{pc1} [V]	E_{pa1} [V]	$E_{1/2}$ [V] (ΔE_p [mV])	E_{pc2} [V]	E_{pa2} [V]	$E_{1/2}$ [V] (ΔE_p [mV])
$[Co(\mathbf{L1})_2]Cl$	−1.23	−1.14	−1.19 (90)	−1.88	−1.79	−1.84 (90)
$[Co(\mathbf{L2})_2]Cl$	−1.24	−1.16	−1.20 (80)	−1.89	−1.81	−1.85 (80)

[a] All voltammograms were recorded in DMF; the potentials are referenced to the Ag/AgCl couple. Conditions: scan rate = 0.1 V/s, compound (1 mM), TBAP (0.1 M), glassy carbon working electrode.

6.2.4 Proton reduction activity of the complexes

For both compounds the electrocatalytic activity was determined for the HER in DMF, using acetic acid as the proton source. In the presence of low acid concentrations (10 eq acid) using complex [Co(**L1**)$_2$]Cl, two irreversible reductive peaks were found at −1.17 and −1.32 V, followed by an obvious catalytic wave at −1.81 V vs Ag/AgCl. The voltammogram of complex [Co(**L2**)$_2$]Cl showed a similar result, showing two irreversible reduction peaks at −1.16 and −1.45 V, followed by a catalytic wave at −1.78 V (Figure 6.4). The first reductive event occurred at slightly more positive potentials than the Co^{III}/Co^{II} reductive event in the absence of acid. A new reduction process seems to be present at a potential that is much more positive than the reductive wave ascribed to the Co^{II}/Co^{I} couple that in the absence of acid is located around −1.8 V.

The CV of a solution of the acid in DMF in the absence of catalyst, the CV of the ligand precursor H_2**L2**Cl in the presence of acid, and the CV of the complex [Co(**L2**)$_2$]Cl are compared in Figure 6.5. The CV of pure acid does not show a significant catalytic current and the CV of the ligand precursor H_2**L2**Cl shows a small reductive wave (discussed in detail in appendix VI). Thus the catalytic current found in the presence of the coordination compound must be related to the cobalt redox couple.

The voltammograms that were obtained for complex [Co(**L2**)$_2$]Cl in varying concentrations of acid are shown in Figure 6.6. The catalytic current increased with increasing concentrations of the acid, and the onset potential of the catalytic peak gradually shifts to more positive potentials. This shift in onset potential indicates that a proton-coupled electron transfer (PCET) process is operative.[7, 19]

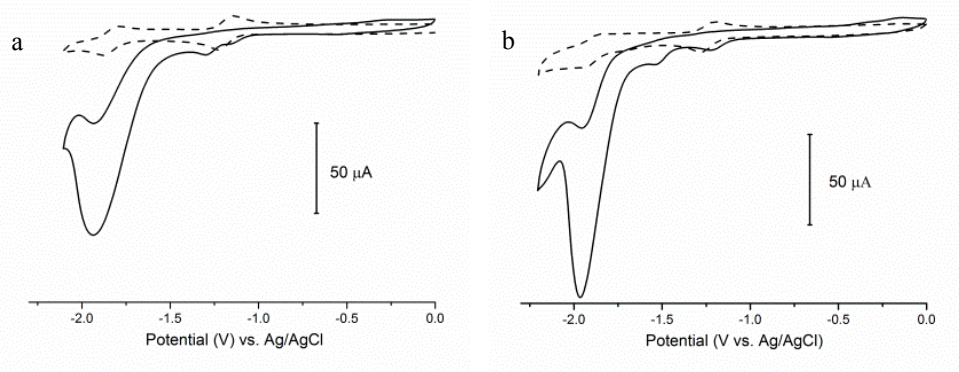

*Figure 6.4. CVs of 1 mM complex [Co(**L1**)$_2$]Cl (a) and [Co(**L2**)$_2$]Cl (b) in absence (dashed line) and in presence (solid line) of 10 mM acetic acid in DMF containing 0.1 M TBAP as electrolyte at scan rate 0.1 V/s, using glassy carbon working electrode.*

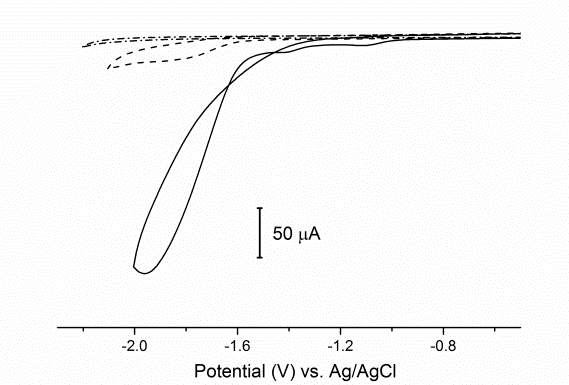

*Figure 6.5. CVs of 30 mM acetic acid (dash-dotted line), 1 mM H_2**L2**Cl in presence of 30 mM acetic acid (dashed line) and 1 mM [Co(**L2**)$_2$]Cl in presence of 30 mM acetic acid (solid line) in DMF containing 0.1 M TBAP as electrolyte at scan rate 0.1 V/s, using glassy-carbon working electrode.*

Plots of i_c/i_p as a function of the square root of the acid concentration are shown in Figure 6.7. A large catalytic current (i_c/i_p = 28 for [Co(**L1**)$_2$]Cl and i_c/i_p = 62 for [Co(**L2**)$_2$]Cl) was observed at 70 eq acid concentration at a scan rate of 0.1 V/s with an overpotential of 940 mV for [Co(**L1**)$_2$]Cl and 830 mV for [Co(**L2**)$_2$]Cl. The complex [Co(**L2**)$_2$]Cl shows asmaller overpotential largely due to the PCET process. For both [Co(**L1**)$_2$]Cl and [Co(**L2**)$_2$]Cl the plot of i_c/i_p show a linear relationship with the square root of acid concentration (Figure 6.7). It indicates the reaction is first-order with respect to acid concentration. Thus, for [Co(**L1**)$_2$]Cl we can use the equation (5) and (6) which show in Chapter 5 to calculate a rate constant k_{obs} of 160 s^{-1} in presence of 70 mM acid at a scan rate of 0.1 V/s. From the plots of k_{obs} versus $[H]^+$, the second-order rate constant was determined to be 2400 M^{-1} s^{-1} (Figure 6.8). Using the same method, for [Co(**L2**)$_2$]Cl we obtained higher rate constant 10500 M^{-1} s^{-1}.

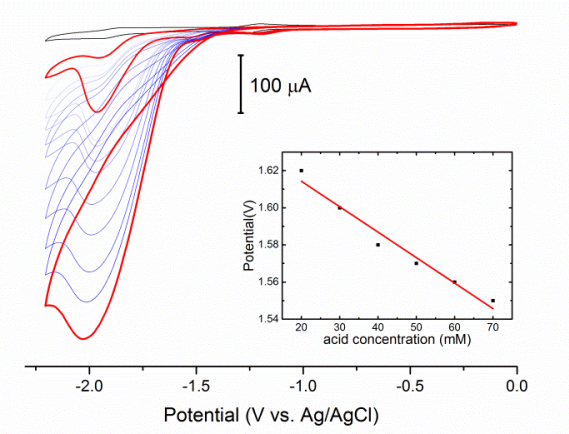

*Figure 6.6. CVs of 1 mM complex [Co(**L2**)$_2$]Cl in presence of various acid concentrations (0 − 70 mM). in DMF containing 0.1 M TBAP as electrolyte. Inset: plot of onset potentials as a function of acid concentration (R^2 = 0.96). Conditions: Scan rate = 0.1 V/s, TBAP (0.1 M), glassy-carbon working electrode.*

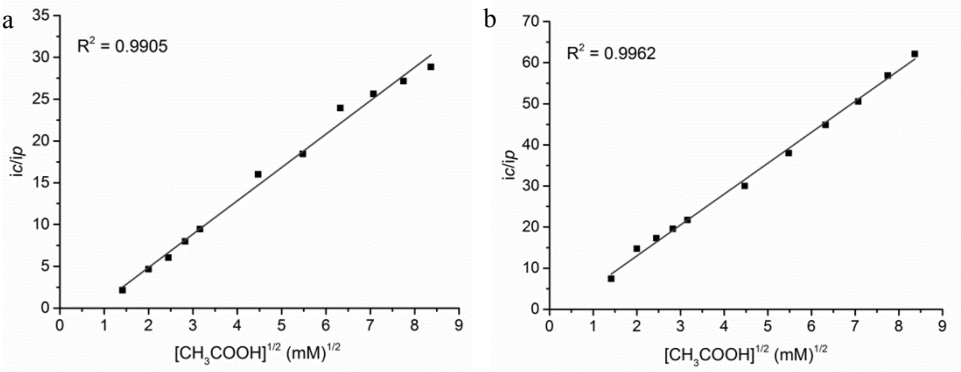

Figure 6.7. Plots of i_c/i_p vs. $[CH_3COOH]^{1/2}$ $(mM)^{1/2}$ for 1 mM $[Co(\mathbf{L1})_2]Cl$ (a) and 1 mM $[Co(\mathbf{L2})_2]Cl$ (b) in presence of various acid concentration in DMF containing 0.1 M TBAP as supporting electrode at 0.1 V/s, using glassy carbon working electrode.

The controlled potential electrolysis (CPE) experiments were carried out to determine which of the two complexes is more active as a electrocatalyst for HER. Hydrogen production was confirmed and quantified using gas chromatography (GC) following CPE at −1.8 V. The faradaic efficiencies were determined to be 77% for $[Co(\mathbf{L1})_2]Cl$ and 82% for $[Co(\mathbf{L2})_2]Cl$. After subtracting the blank (volume of H_2 produced in absence of catalyst, for data treatment see Appendix I) it was deduced that 75 µL and 145 µL H_2 were generated in presence of 1 mM $[Co(\mathbf{L1})_2]Cl$ and $[Co(\mathbf{L2})_2]Cl$, respectively, over 2 h electrolysis, corresponding to 0.6 and 1.2 mol H_2 per mol of catalyst. Although the activity still is rather low, the compound $[Co(\mathbf{L2})_2]Cl$, equipped with free pyridine arms, gave a twice higher catalytic activity in the HER in the same conditions.

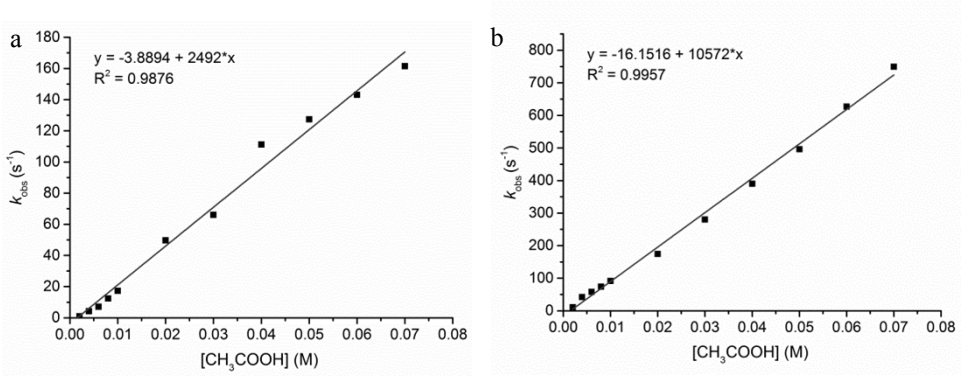

Figure 6.8. Plot of k_{obs} vs. $[CH_3COOH]$ (M) for (a) 1mM $[Co(\mathbf{L1})_2]Cl$ and (b) 1mM $[Co(\mathbf{L1})_2]Cl$ in presence of various acid concentration in DMF containing 0.1 M TBAP as supporting electrode at 0.1 V/s, using glassy carbon working electrode.

6.2.5 Stability of the compounds in acid

In order to investigate how the complexes might interact with protons in electrocatalysis, excess acetic acid-d_4 was added to the complex $[Co(\mathbf{L1})_2]Cl$ or $[Co(\mathbf{L2})_2]Cl$ in acetonitrile-

d_3 (Figure 6.9 and Figure AVI.7). The NMR spectra of [Co(**L1**)$_2$]Cl showed the resonances of the alkyl protons to shift downfield in presence of acid, especially the protons adjacent to the amide (Figure 6.9). The shifts of these alkyl protons are tentatively ascribed to the formation of hydrogen bonds between the amide oxygen and the acid. For complex [Co(**L2**)$_2$]Cl, which equips two free pyridine group, the resonances of alkyl protons were also largely shift down field in presence of acid (Figure AVI.7). It is not only due to the hydrogen bond formation but also due to the protonation of the free pyridine group. The protonation can be confirmed by the EI-MS spectrum of the NMR sample (Figure AVI.8). We found peaks at m/z = 337.5 and 674.7, which assign to [Co(**L2**D)$_2$]$^{2+}$ and [Co(**L2**)(**L2**D)]$^+$ fragments. Meanwhile, no extra peaks appeared upon addition of an excess of acid, indicating both complexes are stable in acidic organic solutions.

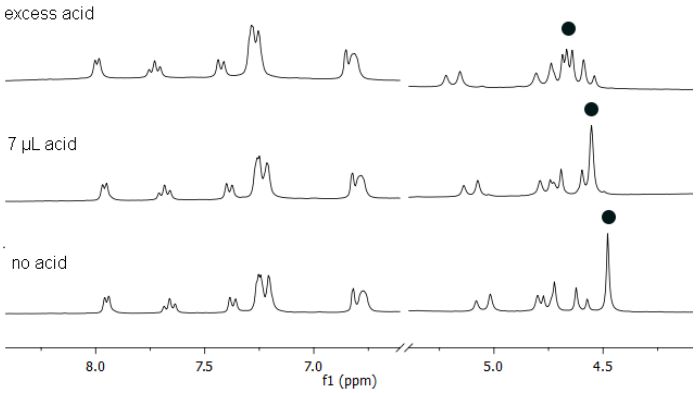

*Figure 6.9. ^{1}H NMR spectra of [Co(**L1**)$_2$]Cl in acetonitrile-d_3 in absence or presence of acetic acid. The black dots refer to the chemical shift of the CH2 between carbene and amide.*

6.3 Conclusion

In this Chapter, the two new cobalt-NHC complexes [Co(**L1**)$_2$]Cl and [Co(**L2**)$_2$]Cl were synthesized. In both octahedral Co^{III} compounds the ligands are coordinated in a meridional tridentate fashion. Although the ligand H$_2$**L2**Cl in combination with Ni^{II} ions forms square-planar coordination compounds with the binding of only one ligand in Chapter 5, we were unable to obtain cobalt compounds with only one ligand coordinated. The strong ligand-field splitting caused by the carbene and amide donor atoms apparently stabilizes a low-spin cobalt(III) compound in an octahedral geometry. More sterically hindering groups should be employed as pendant groups to be able to generate a cobalt(II) compound in a square-planar or 5-coordinate geometry.

Cyclic voltammetry of the two Co-NHC complexes revealed that indeed it is difficult to reduce the Co^{III} center (quite negative Co^{III}/Co^{II} and Co^{II}/Co^{I} redox potentials), which is in agreement with the large ligand-field splitting. The saturated coordination sphere of the cobalt(III) ion in principle makes it difficult to form the cobalt hydride intermediate that is essential in the catalytic proton reduction reaction. However, still both complexes show

electrocatalytic activity in HER using acetic acid as the proton source in dimethylformamide. Large catalytic currents (i_c/i_p = 28 for [Co(**L1**)$_2$]Cl and i_c/i_p = 62 for [Co(**L2**)$_2$]Cl) are observed in the presence of 70 eq acid and at a scan rate of 0.1 V/s with an overpotential of 910 mV for [Co(**L1**)$_2$]Cl and 790 mV for [Co(**L2**)$_2$]Cl. The complex [Co(**L2**)$_2$]Cl shows a smaller overpotential and higher catalytic activity largely due to the PCET process that most likely is facilitated by the presence of free pyridine groups.

6.4 Experimental

6.4.1 Materials

Commercial chemicals were used without further purification. Acetonitrile, tetrahydrofuran, dichloromethane and diethyl ether were obtained from a PureSolv MD5 solvent dispenser. Dry ethanol and dimethylformamide were prepared by adding molecular sieves into commercial anhydrous solvent. The rest commercial solvents were used without further purification. The ligand H_2**L1**Cl was synthesized following a literature method,[12] and the synthesis of the ligand H_2**L2**Cl is described in Chapter 5.

6.4.2 Analytical methods

^{1}H and ^{13}C NMR spectra were recorded on a Bruker 300DPX spectrometer. Mass spectra were obtained using a Finnigan Aqueous Mass Spectrometer (MS) with electro spray ionization (ESI). Cyclic voltammetry was recorded with an Autolab PGstat10 potentiostat controlled by GPES4 software under argon. A 3 mm diameter glassy carbon electrode was used as working electrode and plantium as the counter electrode. The experimental reference electrode was a commercially available Ag/AgCl (E^o = 0.210 V vs. NHE) electrode. Ferrocene was added at the end of each measurement as an internal standard when experiments were carried out in organic solvents; using our conditions the $E_{1/2}$ for the Fc/Fc^+ couple was located at 0.52 V vs. Ag/AgCl, with a ΔE of 90 ~ 110 mV.

Controlled-potential electrolysis (CPE) experiments were carried out in an H-shaped double-compartment cell. A glassy carbon electrode plate with a surface area of 0.07 cm^2 was used as the working electrode for electrolysis. The auxiliary electrode was a platinum gauze electrode. The reference electrode was a commercially available aqueous Ag/AgCl electrode. The sample was bubbled with helium gas for 10 min before measurements and the electrolysis was carried out under helium atmosphere. The solutions in both compartments were constantly stirred during electrolysis experiments. Evolved H_2 gas during electrolysis experiments was quantified by gas chromatography, which was performed on a Shimadzu GC2010 at 35 ºC fitted with a Supelco Carboxen 1010 molecular sieve column. Two parallel experiments were done and the results of two experiments were averaged.

6.4.3 Single crystal X-ray crystallography

For [Co(**L2**)$_2$]Cl, all reflection intensities were measured at 110(2) K using a SuperNova diffractometer (equipped with Atlas detector) with Mo Kα radiation (λ = 0.71073 Å) under the program CrysAlisPro (Version CrysAlisPro 1.171.39.29c, Rigaku OD, 2017). The same program was used to refine the cell dimensions and for data reduction. The structure was solved with the program SHELXS-2014/7 (Sheldrick, 2015) and was refined on F^2 with SHELXL-2014/7 (Sheldrick, 2015).[20] Numerical absorption correction based on gaussian integration over a multifaceted crystal model was applied using CrysAlisPro. The temperature of the data collection was controlled using the system Cryojet (manufactured by Oxford Instruments). The H atoms were placed at calculated positions (unless otherwise specified) using the instructions AFIX 23 or AFIX 43 with isotropic displacement parameters having values 1.2 Ueq of the attached C atoms. The H atoms attached to O1W/O2W/O3W were found from difference Fourier maps (the locations of the H atoms attached to O2W are probably not very accurate as the H atoms might be disordered), and their coordinates were refined freely (the O─H and H…H bond distances were restrained to be 0.84(3) and 1.33(3) Å using the DFIX instruction). The structure is partly disordered.

The fragment N31B-C33B-O32B-C34B-N13B is disordered over two orientations. The occupancy factors of the major component of the disorder refines to 0.519(9). The lattice water molecule O3W has an occupancy factor of 0.5 as it is found on an inversion center.

The crystal that was mounted on the diffractometer was not a single crystal, but rather a composite of two crystals related by a rotation of ca. 1.9° around the reciprocal direction [−0.02 1.00 0.07]. The BASF scale factor refines for 0.0366(18).

For [Co(**L1**)$_2$]PF_6, only the structure of the cations complex could be determined. The counter ions are severely disordered hampering full refinement of the structure.

6.4.4 Complex synthesis

[Co(**L1**)$_2$]Cl:
A Schlenk flask was charged with commercially available anhydrous cobalt(II) acetate (0.35 mmol, 0.06 g), H_2**L1**Cl (0.7 mmol, 0.17 g), K_2CO_3 (2.68 mmol, 0.37 g) and dry DMF (10 mL) under an N_2 atmosphere. The dark brown solution was stirred at room temperature for 2 days. The reaction mixture was filtered to remove the insoluble products and the filtrate was added dropwise into 100 ml diethyl ether. The formed yellow-brown solid was collected by filtration and redissolved in anhydrous acetonitrile. This solution was passed through a short celite column. The solution was concentrated to around 2 mL, and then was added dropwise into diethylether to result in a light brown solid. Single crystals of [Co(**L1**)$_2$]PF_6 for X-ray determination were obtained from anion exchange. The anion exchange was performed by adding a solution of the complex [Co(**L1**)$_2$]Cl in acetonitrile to a boiling acetonitrile solution of NH_4PF_6. Yield: 25% (60 mg). ^{1}H NMR (400 MHz, acetonitrile-d_3) δ 7.95 (d, J = 5.5 Hz, 2H, Py-*H*), 7.66 (td, J = 7.7, 1.4 Hz, 2H, Py-*H*), 7.38 (d, J = 7.8 Hz, 2H, Py-*H*), 7.29 – 7.24 (m, 6H, Ar-*H*), 7.22 (d, J = 7.22 Hz, 2H, Py-*H*), 7.20

(d, J = 5.5 Hz, 2H, $C_{imidazole}$-*H*), 6.82 (d, J = 2.0 Hz, 2H, $C_{imidazole}$-*H*), 6.78 (dd, J = 5.5, 3.7 Hz, 4H, Ar-*H)*, 5.05 (d, J = 19.1 Hz, 2H, Ar-CH*H*-$N_{imidazole}$), 4.77 (d, J = 19.6 Hz, 2H, Ar-CH*H*-$N_{imidazole}$), 4.75 (d, J = 15.2 Hz, 2H, Py-CH*H*-N_{Amide}), 4.60 (d, J = 15.2 Hz, 2H, Py-CH*H*-N_{Amide}), 4.48 (s, 4H, C(O)-CH_2-$N_{imidazole}$). ^{13}C NMR (101 MHz, acetonitrile-d_3) δ = 212.58, 208.75, 208.63, 208.65, 149.67, 139.95, 129.86, 129.16, 128.48, 125.76, 125.51, 125.15, 122.85, 56.02, 55.99, 52.41. ESI-MS found (calculated): $[M–Cl]^+$ *m/z* 669.3 (669.21).

$[Co(\mathbf{L2})_2]Cl$:
A Schlenk flask was charged with anhydrous cobalt(II) acetate (0.85 mmol, 0.15 g), H_2**L2**Cl (0.85 mmol, 0.29 g), K_2CO_3 (3.4 mmol, 0.47 g) and dry CH_3CN (10 mL) under an N_2 atmosphere. To this mixture 2 mL DMF was added. The dark brown suspension was stirred at room temperature for 2 days. The reaction mixture was filtered to remove the insoluble products, and the filtrate was added dropwise into 100 ml diethyl ether. The yellow-brown solid was collected by filtration, redissolved in anhydrous acetonitrile and passed through a short celite column. The solution was concentrated to around 2 mL, and added dropwise into diethyl ether to result in a light brown solid. Single crystals of $[Co(\mathbf{L2})_2]Cl$ for X-ray determination were obtained from a DCM solution of complex in 3 days. Yield: 30% (90 mg). ^{1}H NMR (300 MHz, acetonitrile-d_3) δ 8.42 (dd, J = 17.9, 4.8 Hz, 2H, Py-*H*), 7.90 (d, J = 5.7 Hz, 2H, Py-*H*), 7.76 – 7.62 (m, 4H, Py-*H*), 7.43 (d, J = 7.8 Hz, 2H, Py-*H*), 7.20 (q, J = 7.0 Hz, 4H, Py-*H*), 7.12 (d, J = 1.8 Hz, 2H, $C_{imidazole}$-*H*), 7.02 (d, J = 7.8 Hz, 2H, Py-*H*), 6.87 (d, J = 2.0 Hz, 2H, $C_{imidazole}$-*H*), 5.30 (d, J = 18.8 Hz, 2H, Py-CH*H*-N_{NHC}), 4.98 (d, J = 15.8 Hz, 2H, Py-CH*H*-N_{Amide}), 4.79 (d, J = 15.8 Hz, 2H, Py-C*H*H-N_{Amide}), 4.65 – 4.46 (m, 4H, C(O)-C*H*H-N_{NHC}, Py-C*H*H-$N_{imidazole}$), 4.37 (d, J = 17.0 Hz, 2H, C(O)-CH*H*-$N_{imidazole}$). ^{13}C NMR (75 MHz, acetonitrile-d_3) δ = 170.07, 164.36, 155.26, 150.38, 149.18, 139.87, 138.05, 126.39, 125.26, 124.82, 124.00, 123.26, 122.70, 55.92, 55.78, 53.28. ESI-MS found (calculated): $[M–Cl]^+$ *m/z* 671.1 (671.2).

6.5 Acknowledgements

S. Luo gratefully acknowledges a grant from the Chinese Scholarship Council (no. 201306410011). We thank Mr. J.M.M van Brussel for ESI-MS measurements.

6.6 References

[1] A.D. Wilson, R.K. Shoemaker, A. Miedaner, J.T. Muckerman, D.L. DuBois, M.R. DuBois, *Proc. Natl. Acad. Sci. U. S. A.* 2007, 104, 6951-6956.

[2] J.L. Dempsey, B.S. Brunschwig, J.R. Winkler, H.B. Gray, *Acc. Chem. Res.* 2009, 42, 1995-2004.

[3] P.A. Jacques, V. Artero, J. Pecaut, M. Fontecave, *Proc. Natl. Acad. Sci. U. S. A.* 2009, 106, 20627-20632.

[4] W.K.C. Lo, C.E. Castillo, R. Gueret, J. Fortage, M. Rebarz, M. Sliwa, F. Thomas, C.J. McAdam, G.B. Jameson, D.A. McMorran, J.D. Crowley, M.-N. Collomb, A.G. Blackman, *Inorg. Chem.* 2016, 55, 4564-4581.

[5] P. Zhang, M. Wang, Y. Yang, T. Yao, L. Sun, *Angew. Chem. Int. Ed*. 2014, 53, 13803-13807.
[6] J.W. Jurss, R.S. Khnayzer, J.A. Panetier, K.A. El Roz, E.M. Nichols, M. Head-Gordon, J.R. Long, F.N. Castellano, C.J. Chang, *Chemical Science* 2015, 6, 4954-4972.
[7] P. Zhang, M. Wang, Y. Yang, D. Zheng, K. Han, L. Sun, *Chem. Commun.* 2014, 50, 14153-14156.
[8] M.C. Jahnke, T. Pape, F.E. Hahn, *Eur. J. Inorg. Chem.* 2009, 1960-1969.
[9] C. Fliedel, P. Braunstein, *J. Organomet. Chem.* 2014, 751, 286-300.
[10] K. Kawano, K. Yamauchi, K. Sakai, *Chem. Commun.* 2014, 50, 9872-9875.
[11] M. van der Meer, E. Glais, I. Siewert, B. Sarkar, *Angew. Chem. Int. Ed.* 2015, 54, 13792-13795.
[12] J.-Y. Lee, J.-Y. Lee, Y.-Y. Chang, C.-H. Hu, N.M. Wang, H.M. Lee, *Organometallics* 2015, 34, 4359-4368.
[13] Z. Xi, B. Liu, C. Lu, W. Chen, *Dalton Trans.* 2009, 7008-7014.
[14] Z. Mo, Y. Li, H.K. Lee, L. Deng, *Organometallics* 2011, 30, 4687-4694.
[15] F. Hering, J.H.J. Berthel, K. Lubitz, U.S.D. Paul, H. Schneider, M. Härterich, U. Radius, *Organometallics* 2016, 35, 2806-2821.
[16] A. Massard, P. Braunstein, A.A. Danopoulos, S. Choua, P. Rabu, *Organometallics* 2015, 34, 2429-2438.
[17] S. Dürr, D. Ertler, U. Radius, *Inorg. Chem.* 2012, 51, 3904-3909.
[18] S. Saha, M. Kaur, K. Singh, J.K. Bera, *J. Organomet. Chem.* 2016, 812, 87-94.
[19] R.M. Bullock, A.M. Appel, M.L. Helm, *Chem. Commun.* 2014, 50, 3125-3143.
[20] G.M. Sheldrick, *Acta Cryst. C* 2015, 71, 3-8.